Research Article

Thermodynamics and kinetics of the removal of methylene blue from aqueous solution by raw kaolin

Achraf Harrou[1] · Elkhadir Gharibi[1] · Hicham Nasri[2] · Meriam El Ouahabi[3]

Abstract

Remediation of contaminated water with organic dyes originated from variety of industrial processes deserves increased attention. Raw clay is an effective low-cost and eco-environmentally friendly adsorbent for the removal of methylene blue (MB) from solution. This study aims to determine kinetics and thermodynamics of MB adsorption onto raw kaolin clays (halloysite and kaolinite/illite) from northeast of Morocco. The apportion capacity of the two kaolin clays to adsorb the MB dye by varying temperature and pH conditions was studied. The thermodynamic parameters show that the sorption of MB is spontaneous and endothermic for halloysite-rich clay, whereas adsorption onto kaolinite/illite is inhibited by electrostatic exothermic effects and the sorption is thermodynamically unfavorable. The kinetic study showed that the adsorption capacity of MB on halloysite is greater than on kaolinite. The intraparticle diffusion process controls the adsorption reaction, and the kinetic is more important for halloysite.

1 Introduction

Recently, numerous approaches have been studied for the development of low-cost and effective adsorbents, including clay minerals, zeolites, siliceous material, biosorbents and agricultural wastes and industrial by-products [1–7]. Adsorbents with high surface area are requested, such as mesoporous [8, 9] and microporous materials [10, 11], carbon nanotubes [12] and titania nanotubes [13]. In particular, polydopamine (PDA) microspheres, poly(cyclotriphosphazene-co-4,4'-sulfonyldiphenol) (PZS) nanospheres, synthesized by oxidative polymerization or by an in situ template method, were successfully used as a high-efficiency adsorbent for the removal of a cationic dye (methylene blue) from aqueous solution [14–16].

Clay minerals are effective adsorbents, due to their high specific surface area and high cation exchange capacity

and their shaper price [17]. Raw kaolin as a low-cost adsorbent was studied for removal of methylene blue from aqueous solutions [e.g., 18, 19].

Kaolin is the most abundant mineral in sediments, and its origin is residual or hydrothermal [20, 21]. Kaolin has different properties depending on several factors including the geological conditions under which the kaolin was formed, the mineralogical composition and the physical and chemical properties. Kaolinite and halloysite are the main mineral phases of the kaolin group $(Al_2Si_2O_{10}(OH)_4)$, which consists of dioctahedral 1:1 layers.

Kaolinite is mainly present as plates and lamellar aggregates, with a very low cation exchange capacity (from 1 to 2 meq/100 g) because of the low isomorphous substitution in both the tetrahedral and octahedral sheets [22]. Its specific surface area is very small (between 8 and 12 $m^2\,g^{-1}$).

✉ Meriam El Ouahabi, meriam.elouahabi@uliege.be | [1]Laboratory of Mineral and Analytical Solid Chemistry, Department of Chemistry, Faculty of Sciences, Mohamed I University, P.O. Box 60000, Oujda, Morocco. [2]Applied Geosciences Laboratory, Department of Geology, Faculty of Sciences, Mohamed I University, P.O. Box 60000, Oujda, Morocco. [3]UR Argile, Géochimie et Environnement sédimentaires (AGEs), Department de Geology, Quartier Agora, Bâtiment B18, University of Liège, Allée du six Aout, 14, Sart-Tilman, 4000 Liège, Belgium.

Halloysite nanotube (HNTs) is typically hydrated and contains two H_2O molecules per unit cell, and the thickness of the 1:1 layer plus the interlayer is equal to ~ 10 Å. Hydrated halloysite is unstable and readily and irreversibly transforms into a dehydrated state at ~ 7 Å [23]. Halloysite has a substantially different morphology than kaolinite, where microtubular structure is the most frequent form.

Halloysite is mainly derived from long-term weathering of amorphous silicate, which remained in small amount as relicts associated with raw halloysite [24, 25]. Similar to the carbon nanotube, halloysite is of particular importance due to its tubular morphology of 500–1000 nm in length and 10–100 nm in inner diameter [26]. Halloysite has a larger cation exchange capacity than kaolinite which stands at 5 meq/100 g [21]. The HNTs find several applications such as ceramic, support for catalysts and other functional materials [27, 28]. Recently, raw halloysite was successfully tested as adsorbents for removal of dyes, heavy metals and pollutants from aqueous solutions [e.g., 29–31].

It is known that raw kaolin is mostly heterogeneous and contains other clay phases (e.g., illite, smectite), which can influence the absorption behavior of cationic dyes. This study aims to evaluate the suitability of raw kaolin clays as low-cost adsorbents for cationic dye from aqueous solution under operational conditions, such as dye concentration, pH and the adsorbent dosage. A comparison between kinetics and mechanism of removal of methylene blue by adsorption on raw halloysite and kaolinite is a further the aim of this study.

2 Materials and methods

2.1 Raw materials

The HNTs used in this study were obtained from the Hed Beni Chiker deposit located in the northeast of Morocco in the Nador area. Halloysite belongs to the Neogene basin, located at the base of the Messinian series, between marl with a reef limestone and volcanic sandstone from the Gourougou volcano. Halloysite has a volcanic origin through the hydrothermal circulation of fluid rich in sulfur.

Kaolinite-rich clay was obtained from the Glib Naam deposit located in the Jerada area in the northeast of Morocco (N: 34°23′30.9″, W: 2°00′44.1″). This kaolin is derived from the chemical alteration favored by a humid climate and active tectonics facilitating the drainage of water and the hydrothermal alteration of the Beni-Snassene granodiorite [32].

Halloysite-rich clay was treated by hydrochloric acid solution (0.05 N) to eliminate organic matter and carbonate. Afterward, the supernatant was centrifuged to remove the liquid phase and wash by distilling water. The clay obtained is dried in the oven for 24 h. The treated halloysite was grinded (200 μm) to be used for characterization tests and adsorption properties [33]. Kaolinite was grained (200 μm) without any chemical pretreatment.

2.2 Analysis and characterization

2.2.1 Physicochemical properties of clays

Powder XRD patterns were measured for kaolinite-rich clay and halloysite samples with a Shimadzu XRD 6100 diffractometer, equipped with a Cu X-ray tube, operating at 40 kV and 30 mA, in the 4°–80° 2θ range, step size 0.02 and 1-min counts per step.

Differential thermal analysis (DTA) and thermogravimetric analysis (TG) methods were performed on both raw clay samples using a SHIMADZU instrument (DTG-60 H). The experiment was performed on 5–10 mg of sample using a temperature range from 35 to 1000 °C with a heating rate of 10 °C/min.

Infrared spectroscopy (IR) was performed on both the clay samples. Thin pellets were prepared with a mixture of 95% of KBr and 5% of the clay sample. The FTIR spectra were carried out using a SHIMADZU Fourier transform FTIR-8400 spectrophotometer in a wavelength range of 400–4000 cm^{-1}.

Cation exchange capacity (CEC) and specific surface area (SSA) were estimated using the copper ethylene diamine $((EDA)_2CuCl_2)$ method [34, 35]. The CEC was calculated from the quantity of $(EDA)_2^{2+}$ adsorbed by the clay: the amount initially added to the clay suspension minus the amount remaining in the supernatant solution after adsorption and centrifugation.

Scanning electron microscope (SEM) observations were performed on both raw halloysite and kaolinite clays by using a Quanta-200 scanning electron microscope (CNRST, Rabat, Morocco). In situ chemical composition was determined by energy-dispersive X-ray spectroscopy (EDX). The images were obtained with a secondary electron detector at a voltage of 10 kV on gold-sputtered powdered samples.

2.2.2 Adsorption kinetics

Adsorption of methylene blue was carried out in raw kaolinite-rich clay and halloysite. The effect of contact time on the amount of the adsorbed dye was investigated by various concentrations ($[MB_{ini}] = 5, 10, 20$ and 30 mg/l) and at different temperatures (30, 40, 50 and 60 °C). A 25 mg of HNTs and kaolinite were mixed with 25 ml of MB solution with known initial concentration at different pH 3, 5, 7, 9 and 11. At the end of the adsorption period, the solution was centrifuged for 5 min. Thereafter, the MB

concentration in the supernatant solution was analyzed using a UV spectrophotometer (Macy UV-1100) at a maximum absorbance of 662 nm.

The amount of MB adsorbed (mg/g) (Q), onto clay, was calculated from the mass balance equation as follows:

$$Q(mg/g) = (C_0 - C) \cdot V°/m$$

where C_0 and C are the initial and equilibrium liquid-phase concentrations of MB (mg/l), respectively, V is the volume of MB solution and m is the mass of the clay used (g) [36, 37].

2.2.3 Thermodynamic study

The thermodynamics parameters that must be considered to determine the process are changes in the standard enthalpy ($\Delta H°$), standard entropy ($\Delta S°$) and free standard energy ($\Delta G°$) due to the transfer of the unit from dissolved body from the solution at the solid–liquid interface [38, 39]. The values of $\Delta H°$ and $\Delta S°$ were calculated using the following van't Hoff equation:

$$K_d = Q_e/C_e = e^{(\Delta S°/R - \Delta\Delta°/RT)} \quad \ln K_d = \Delta S°/R - \Delta H°/RT$$

where R is the gas constant ($R = 8.314$ J.mol^{-1}.K^{-1}), T is absolute temperature of solution (K), K_d distribution coefficient, Q_e is the amount adsorbed at equilibrium (mg g^{-1}) and C_e is the equilibrium concentration (mg L^{-1}). The values of $\Delta H°$ and $\Delta S°$ were calculated from the slope and interception of the plot of ln K_d function. $\Delta G°$ can be calculated using the following equation:

$$\Delta G° = \Delta H° - T\Delta S° = -RT \ln K_d$$

These thermodynamic estimates can offer insight into the type and mechanism of an adsorption process.

3 Results and discussion

3.1 Physicochemical composition of raw halloysite and kaolinite

The mineralogical composition (XRD) and microstructure (SEM) of raw halloysite and kaolinite rich samples are illustrated in Fig. 1. The raw HNTs sample is a 7 Å halloysite associated with small quantities of tridymite (SiO_2), cristobalite (SiO_2), gibbsite ($Al(OH)_3$) and alunite ($KAl_3(SO_4)_2(OH)_6$). Raw halloysite contains impurities as quartz, muscovite, feldspar, smectite and kaolinite, as is the case for Thailand and China halloysites [40–42]. SEM image shows tubular structure of halloysite (Fig. 1).

Specific surface area of this halloysite is 70.90 m^2/g, and its cation exchange capacity is 18 meq/100 g.

Raw kaolinite sample contains accessory phases as illite, plagioclase, pyroxene (augite) and quartz. SEM images show that kaolinite and illite particles are mostly altered (Fig. 1). SSA of kaolinite-rich clay is 6.19 m^2/g and its CEC value is 7.6 meq/100 g.

Unlike raw kaolinite-rich clay, raw HNTs underwent a dehydration process of the interlayer water due to the occurrence of the endothermic peak at about 310 °C (Fig. 2). In addition, a loss on mass of 2.8% occurs at about 100 °C, which is attributed to the loss of the surface adsorbed water [25]. These results indicated that halloysite adsorbs water molecules both on surface and lumen space of the nanotubes. The occurrence of a second mass loss implies a further increase in the adsorbed water amount for halloysite. However, raw kaolinite did not display any endothermic peak below 500 °C for (Fig. 2). The mass loss at 550 °C for both clays is attributed to dehydroxylation of kaolinite and halloysite on metakaolin and metahalloysite, respectively. The later loses more weight (− 9.3%) than kaolinite (− 5.6%). The abundant interwall spaces of HNTs accommodated more water molecules than kaolinite.

IR spectra of halloysite shows several bands around 3694; 3622; 3554; 3527; 1094; 1033; 1012; 941: 913; 692; 650; 562; 540; 471; and 432 cm^{-1} (Fig. 3). The observed bands at 1033 cm^{-1} and 3695 cm^{-1} are attributed to the Si–O-Si vibration and Al–OH vibration of halloysite, respectively [43]. The occurrence of the 3527 cm^{-1} and 3454 cm^{-1} bands in raw halloysite sample (Fig. 3) indicates the presence of whole water contained in the hydrated interlayers of halloysite [43].

For kaolinite-rich clay sample, the band at 3622 cm^{-1} is related to an inner hydroxyl stretch with its vector orientation near to the (001) plane. This inner hydroxyl group results from bonding between a proton and an oxygen that is also coordinated to Al^{3+} in an octahedral site.

Kaolinite and halloysite samples show 3350–3650 cm^{-1} broad absorption bands observed are caused by the O–H stretching vibration of the Si–OH bands and HO–H vibration of the H$_2$O adsorbed on silica surface (Fig. 3). In addition, both clays show the occurrence of 937 cm^{-1} band due to plane bending vibrations of the surface hydroxyl groups [44]. Compared to kaolinite, the water hydroxyl deformation of halloysite is sharper and stronger since more interlayer bonded water was adsorbed on the surface of halloysite. The 3454 cm^{-1} band in halloysite was sharper and stronger than kaolinite (Fig. 3) indicating that the water hydroxyl deformation of halloysite is more important and since more interlayer bonded water was adsorbed on the surface of halloysite.
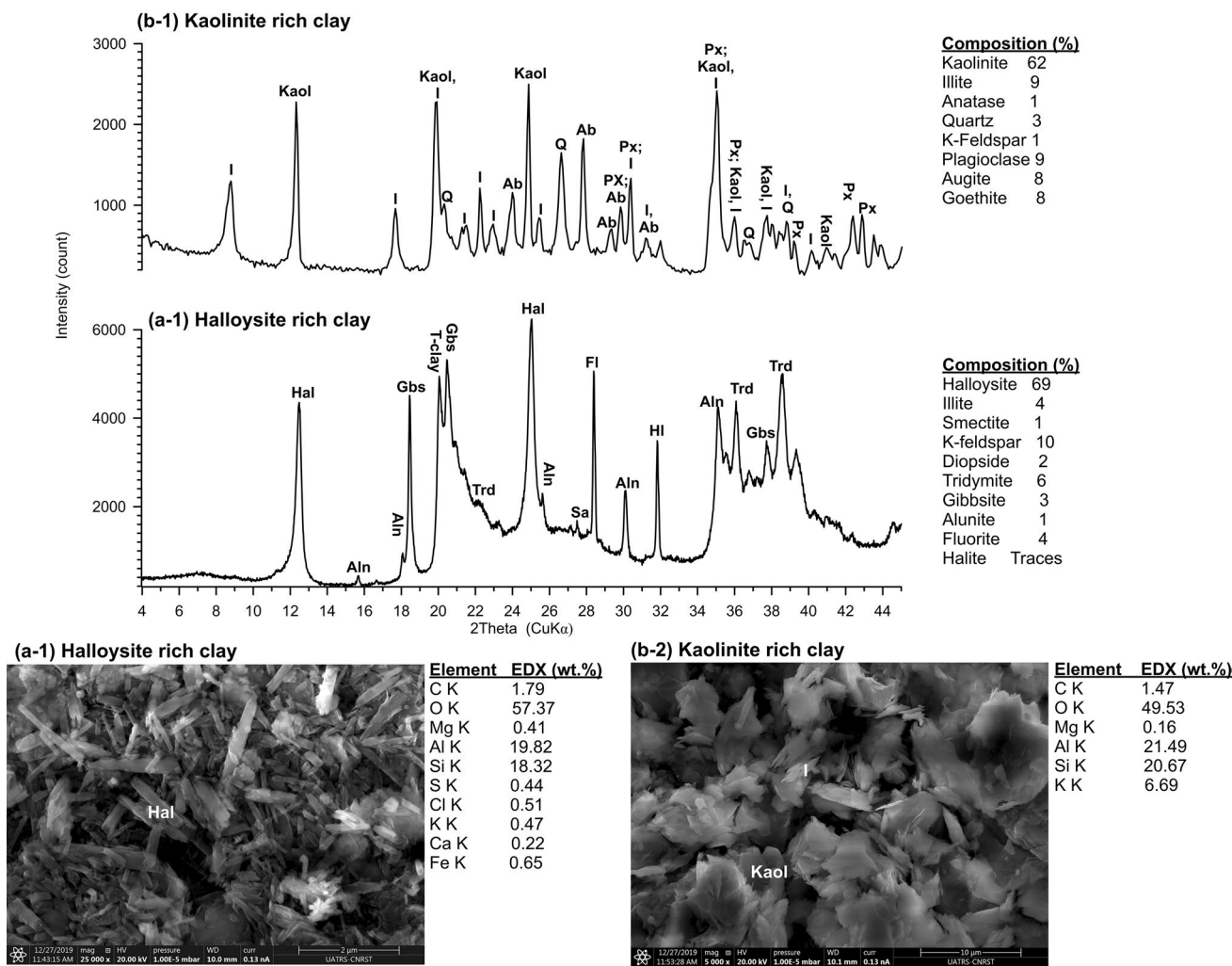
Fig. 1 Mineralogical composition and XRD patterns of raw halloysite (**a-1**) and raw kaolinite samples (**b-2**). **a-2**, **b-2** show SEM images and chemical composition (EDX) of raw halloysite and raw kaolinite-rich clay, respectively. *Hal* halloysite, *Aln* alunite, *Gbs* gibbsite, *Trd* tridymite, *Hl* halite, *Sa* sanidine (K-feldspar), *Fl* fluorite, *I* illite, *Kaol* kaolinite, *Px* pyroxene (augite), *Ab* albite, *Q* quartz

3.2 Adsorption rates

Adsorption rates were investigated using the values of adsorbed dye at different initial MB concentrations, pHs and temperatures in terms of time of reaction.

The effect of initial dye concentration and contact time on the removal rate of MB by HNTs and kaolinite is shown in Fig. 4. The adsorption rate increases with increasing initial dye concentration for HNTs and kaolinite. The results show that the adsorption is rapid during the first 5 min and reached saturation at about 20 min for both clays. The equilibrium was attained at 30 min. The amount of the adsorbed MB onto HNTs was greater than onto kaolinite for different initial MB concentrations. Halloysite absorption rate is similar to sepiolite values [45].

pH is one of the most important factors which controls the adsorption extent of dyes on clay surfaces. The adsorption behavior of the dyes on HNTs and kaolinite was studied over a wide pH range of 3–11 (Fig. 4). The kinetic of adsorption on halloysite is greater than on kaolinite.

The adsorption of these charged dyes onto the adsorbent surface is primarily influenced by the surface charge on the adsorbent which in turn is influenced by the solution pH. The addition of H^+ cations to low pH values causes neutralization of the negative charge on clay surface, which disadvantages the adsorption of positively charged MB molecules.

For halloysite-rich clay, when the pH increases, the adsorption rate, very important at low pH, increases until a pH 9 and then stabilizes. At pH of 6–7, HNTs have a negative charge, where the surface charge becomes positive at pH of 8.5 5 [46]. The positive charge on the surface of HNTs blocks the adsorption of the cationic dye, which allows its stabilization at pH greater than 9.
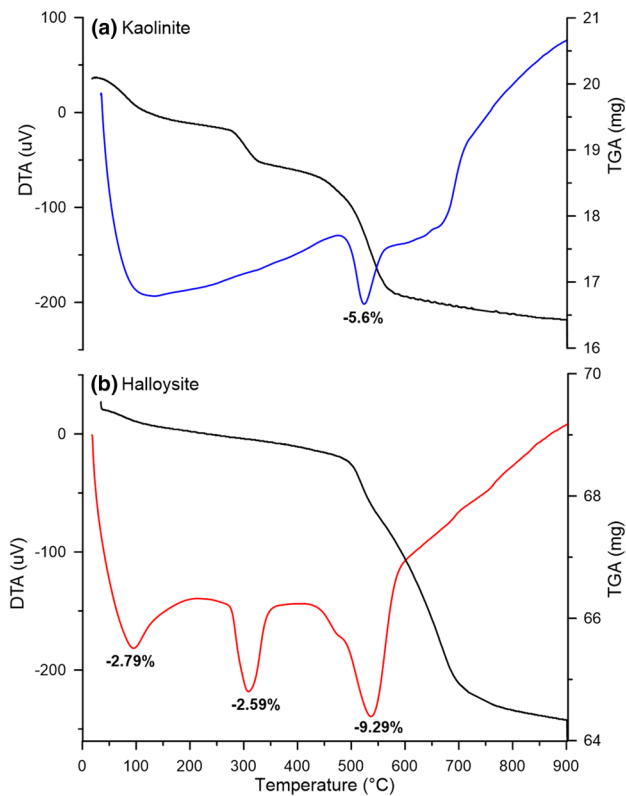
Fig. 2 Thermogravimetric analysis and differential thermal analysis of adsorption of MB onto halloysite (**a**) and kaolinite (**b**)

For kaolinite, at pH ranging from 3 to 5, the adsorption rate increases but diminishes thereafter and increases again from pH 9. The observed increase between pH 3 and

pH 5 is due to the absence of coagulation of kaolinite and illite particles, which is very important at pH 5.8. However, when pH is increased above 5.8, the coagulation rates are greatly reduced [47]. The adsorption process is an intraparticular diffusion as will be demonstrated later.

pH from 5 to 9, (pH < pH$_{PZC\ edge}$) the oppositely charged T face and O face and edge regions are emerged, thus resulting in a decrease in MB adsorption. Alkaline conditions cause a sudden decrease in pH and then hydrolyze of kaolinite and illite, forming an amorphous gel. The proton production produced after this short reaction time comes from gel dissolution [48]. The pH drop is probably a complex surface reaction formed by the hydration of the structural hydroxyls at the surface or the dangling oxygens at the solid borders [49]. For the pH above 5.5, two successive deprotonations occur in kaolinite surface at pH ~ 5.5 and ~ 9 [48]. So, the adsorption of MB increases when the pH exceeds 9 and decreases when the pH values are greater than 5.5.

3.3 Thermodynamic analyses

MB adsorption onto HNTs and onto kaolinite at different temperatures is shown in Table 1. The initial pH was selected as 5.64, and the initial concentration of MB was 20 mg/L. The MB adsorption capacity presents a significant increasing trend with the rise in temperature (20–60 °C) for kaolinite. Nevertheless, the $\Delta G°$ values of the adsorption of MB dye onto HNTs are negative from − 2598.3 kj mol^{-1} at 20 °C to − 2951.28 kj mol^{-1} at 60 °C, thus confirming that halloysite adsorption is spontaneous.

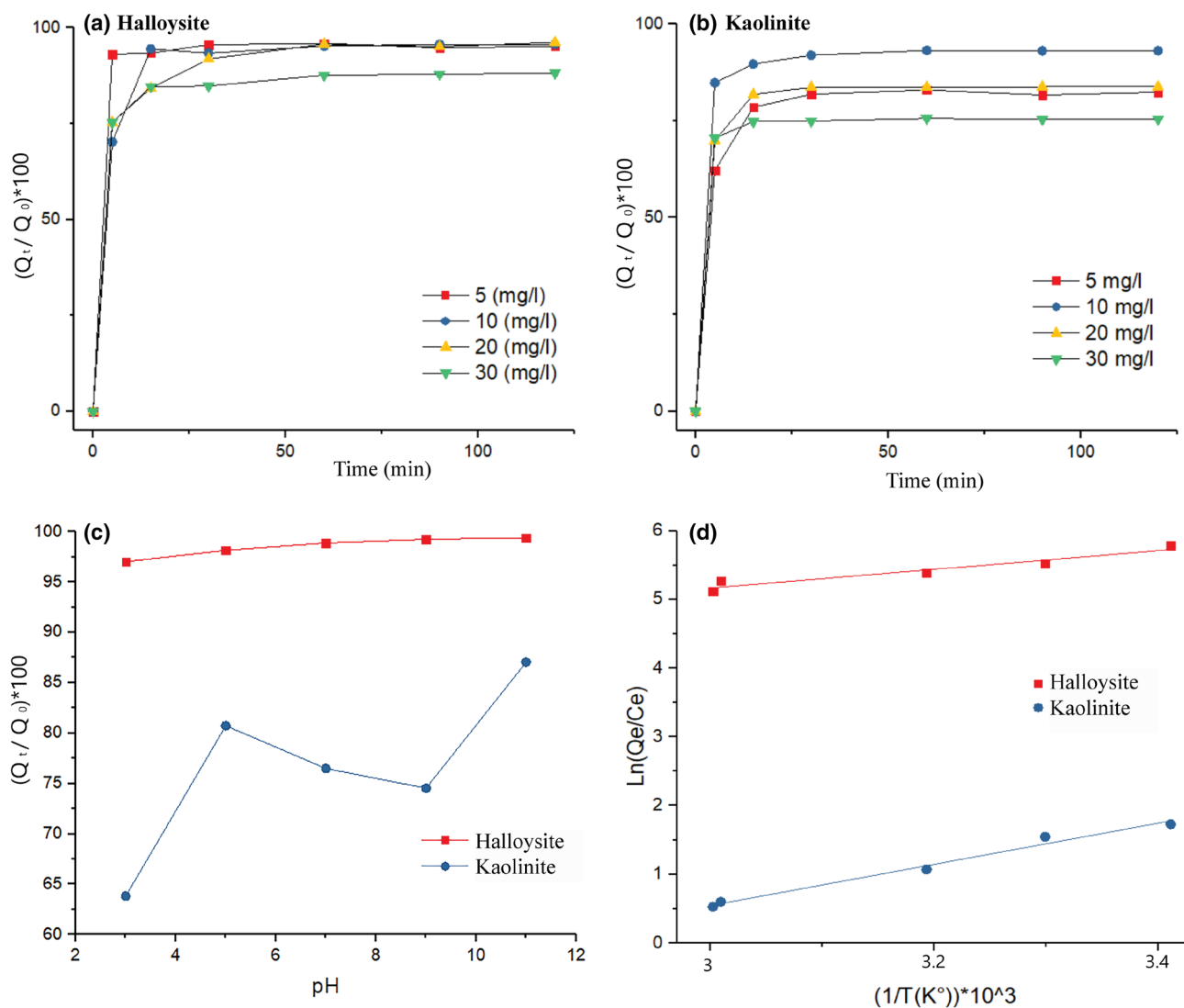**Fig. 3** Infrared spectra of halloysite and kaolinite samples
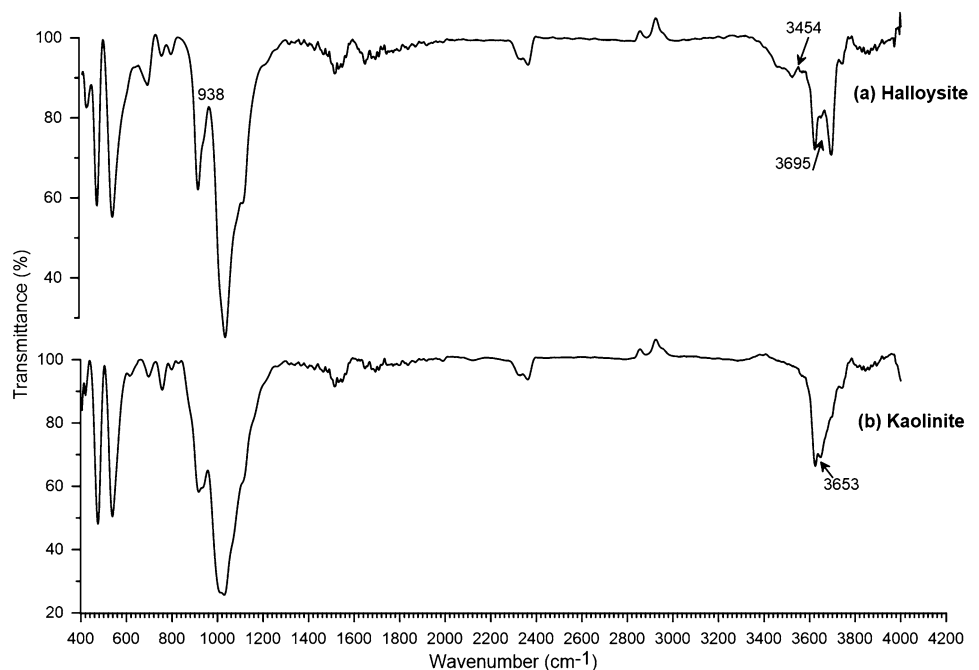
Fig. 4 The effect of concentration (**a**, **b**) and pH (**c**) on the removal of methylene blue onto halloysite and kaolinite-rich clay. **d** Thermodynamic results of the adsorbed MB onto both clays

Table 1 Thermodynamic parameters for MB adsorbed by halloysite and kaolinite

	Halloysite	Kaolinite
$\Delta H°$ (kj mol^{-1})	8.82	-70.20
$\Delta S°$ (kj mol^{-1} K^{-1})	-11.37	-24.91
T (°C)	ΔG(kj mol^{-1})	ΔG(kj mol^{-1})
20	-2598.3	20,604.63
30	-2686.5	21,306.65
40	-2774.79	22,008.67
50	-2863.04	22710.69
60	-2951.28	23412.71

It has been demonstrated that the driving force of adsorption is greater and the adsorption capacity is higher

when $\Delta G°$ value is less than 0 [50]. On the other hand, the $\Delta G°$ (20,604.63 kj mol^{-1}) of the adsorption of MB onto kaolinite is positive at 20 °C, confirming that this adsorption is inhibited by the patch-wise charge heterogeneity. Results obtained on kaolinite-illite-rich clay by Omer et al. [51] showed that the enthalpy of adsorption of MB is slightly positive and the adsorption of MB was not favored at high temperatures.

The average values of $\Delta H°$ of HNTs and kaolinite are 8.8246 kj mol^{-1} and -70.2020 kj mol^{-1}, respectively. Studies have reported that the $\Delta H°$ of physisorption is smaller than 40 kj mol^{-1} [52], involving that MB adsorption onto the two clays is a physisorption process. At pH 5.68, adsorption of MB on halloysite is an endothermic process. According to thermodynamic values for kaolinite-rich clay, the sorption seems to have prevented the dissolution of

the amorphous gel and the production of protons on the surface, which repels by exothermic electrostatic effect of the MB cations.

As reported in Table 1, the negative $\Delta S°$ for halloysite indicates that the degrees of freedom decrease at the adsorbate–adsorbent interface during the adsorption process. For kaolinite, the rise in temperature causes a slight increase in the proton surface charge between pH 4 and 9 [53], which increases the electrostatic repulsion of the cationic dye.

3.4 Adsorption kinetics

3.4.1 The pseudo-first-order kinetic model

The pseudo-first-order kinetic model has been widely used to predict dye adsorption kinetics. Lagergren suggested a pseudo-first-order model [54]:

$$Ln(Q_e - Q_t) = LnQ_e - k_1 * t$$

where q_t is the adsorbed amount at time t (mg/g) and k_1 is the equilibrium rate constant of pseudo-first-order adsorption (min^{-1}). The values $Ln(Q_e - Q_t)$ were calculated from the kinetic data. It was observed (Fig. 5) that the correlation coefficients (Table 2) were lower for all concentrations of the added MB. Therefore, the pseudo-first-order model is not applicable to predict the kinetics of the MB adsorption onto HNTs and kaolinite.

3.4.2 The pseudo-second-order kinetic model

The pseudo-second-order kinetic model was used to explore the adsorption mechanism. This model takes into account the adsorbed quantities that will enable us to determine the reactor volume. The mathematical expression of this model is as follows [55]:

$$dQ/dt = K_2(Q_e - Q_t)$$

where K_2 is the pseudo-second-order rate constant of adsorption (g mg^{-1} min^{-1}), Q_t is the adsorption capacity at the moment t and Q_e is the adsorption capacity at equilibrium. By integrating the previous equation, t/Q_t can be expressed as the following:

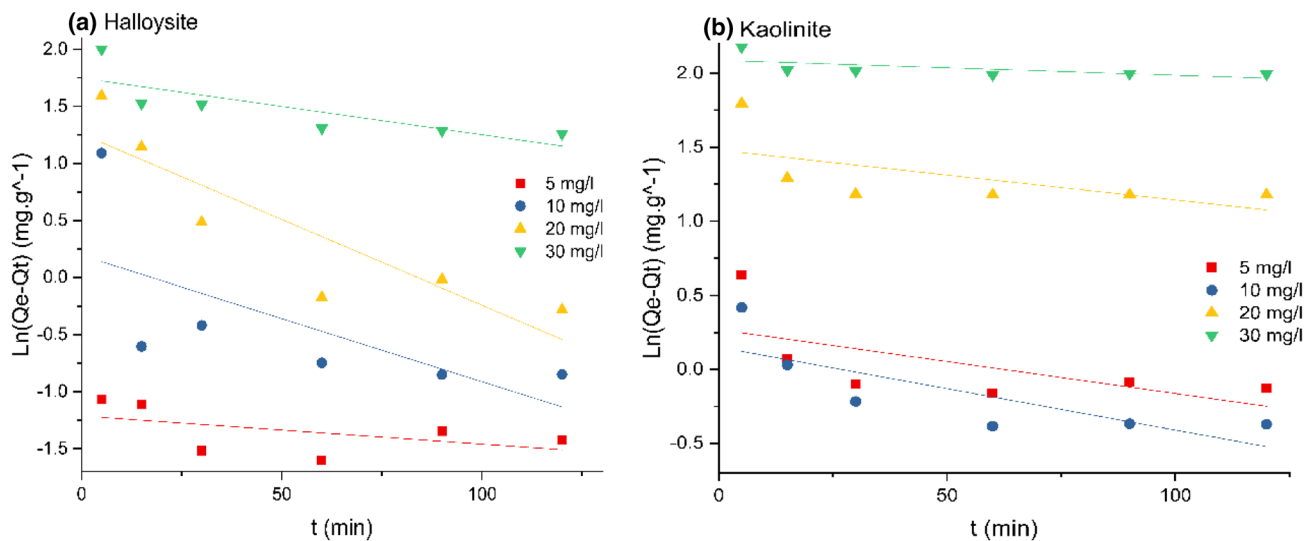$$t/Q_t = 1/(K_2 * Q_e^2) + t/Q_e$$

Fig. 5 Pseudo-first-order kinetic model for adsorption of methylene blue on halloysite and kaolinite-rich clay

Table 2 The result of application of pseudo-first-order kinetic model for adsorption of MB by halloysite and kaolinite

[MB]$_{ini}$ (mg/L)	Halloysite				Kaolinite			
	K_1 (cm^{-1})	Q_e(th)	Q_e(exp)	R^2	K_1 (cm^{-1})	Q_e (th)	Q_e (exp)	R^2
5	0.002	3.01	4.98	0.26	0.004	0.68	4.76	0.41
10	0.011	2.67	9.71	0.45	0.006	2.79	9.57	0.63
20	0.015	10.11	19.53	0.78	0.003	8.09	19.24	0.38
30	0.005	18.54	29.13	0.65	0.001	13.21	26.47	0.40

The curves of t/Q_t versus t are given in Fig. 6. The calculated Q_e and K_2 correspond to linear regression correlation, and the R^2 values are represented in Table 3. The linear plots of t/Q_t versus t are in good agreement with experimental Q_e values. The correlation coefficients (R^2) for the second-order kinetics model are greater than

0.99, indicating the applicability of this kinetics equation and the second-order nature of the adsorption process of methylene blue onto raw HLNs and kaolinite/illite. It is found that for both adsorptions the rate constant K_2 decreases with the increase in the concentration of MB initially introduced.
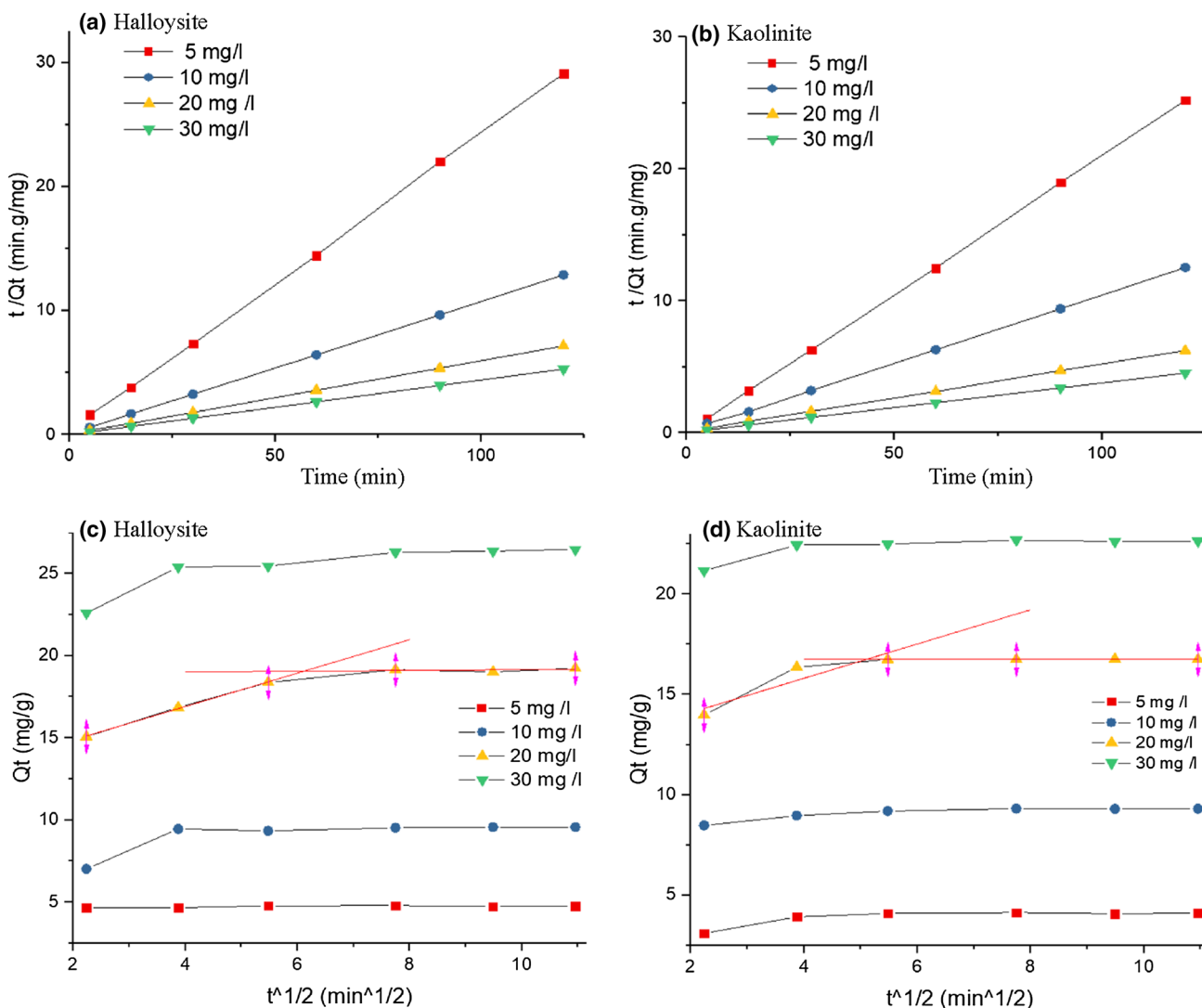

Fig. 6 Pseudo-second-order kinetic model (**a**, **b**) and intraparticle diffusion kinetic model (**d**, **c**) for adsorption of methylene blue on halloysite and kaolinite-rich clay

Table 3 The result of application of pseudo-second-order kinetic model for adsorption of MB by halloysite and kaolinite

[MB]$_{ini}$ (mg/L)	Halloysite				Kaolinite			
	Q_e (th)	K_2	R^2	Q_e (exp)	Q_e (th)	K_2	R^2	Q_e (exp)
5	4.98	1.05	0.99	4.98	4.76	8.82	0.99	4.76
10	9.73	0.32	0.99	9.71	9.64	0.14	0.99	9.57
20	19.68	0.05	0.99	19.53	19.38	0.04	0.99	19.24
30	29.76	0.01	0.99	29.13	26.59	0.04	0.99	26.47

3.4.3 Error functions

The error functions such as hybrid fractional error function (HYBRID), Marquardt's percent standard deviation (MPSD), the average relative error (ARE), sum of the errors squared (ERRSQ) and sum of the absolute errors (EABS); standard deviation of relative errors (SRE); and nonlinear chi-square test (X^2) were determined for different concentrations for MB to minimize the error distribution between the experimental equilibrium data and the pseudo-kinetics models [56] (Table 4).

Based on Fig. 6, the MPSD function is found to be a better option to minimize the error distribution between the experimental and predicted pseudo-kinetics models.

3.4.4 Intraparticle diffusion

The adsorbed elements are most likely transported from the solution to the solid phase by an intraparticular diffusion process, which is often the limiting step in various adsorption processes. The intraparticle diffusion model describes adsorption processes, where the rate of adsorption depends on the speed at which adsorbate diffuses toward adsorbent, according to the following equation [57]:

$$Q_t = k_{id} \sqrt{t} + C$$

where Q_t is the amount of MB adsorbed onto the raw clays at the moment t, C is the intercept and k_{id} is the intraparticle diffusion rate constant (mol/g min$^{1/2}$).

Multilinear plots of intraparticle diffusion process of MB adsorption onto the HNTs nanotubes and kaolinite indicate the occurrence of two steps (Fig. 6). The two steps correspond to the diffusion of MB molecules from solution to the external surfaces of clay and intraparticle diffusion of MB molecules through the clay pores. The values of intercept (Table 5) provide information about the boundary layer thickness, i.e., the larger the intercept, the greater is the boundary layer effect. The obtained values suggest that the intraparticle diffusion is not the rate-limiting step and other mechanisms may play an important role. Ki$_1$ values are larger than Ki$_2$, indicating that diffusion process is rapid while intraparticle diffusion is a gradual. In addition,

Table 4 The error functions of application of both pseudo-first-order and pseudo-second-order kinetic models onto the adsorption of MB onto halloysite and kaolinite

Raw clays	[MB]$_0$ (mg/l)	ERRSQ	X^2	EABS	ARE	SRE	HYBRID	MPSD
Pseudo-first-order kinetic model								
Kaolinite	5	1.348E−05	2.879E−06	0.005	0.019	0.022	7.199E−05	0.039
	10	0.438	0.046	1.046	1.838	2.030	1.155	3.488
	20	0.788	0.050	1.521	1.549	1.659	1.254	2.831
	30	0.682	0.027	1.434	0.973	1.008	0.692	1.677
Halloysite	5	1.981E−06	5.952E−07	0.002	0.012	0.013	1.488E−05	0.021
	10	3.534E−05	3.953E−06	0.011	0.021	0.025	9.882E−05	0.033
	20	0.001	6.369E−05	0.045	0.050	0.064	0.001	0.105
	30	0.347	0.016	0.927	0.710	0.840	0.403	1.370
Pseudo-second-order kinetic model								
Kaolinite	5	0.011	0.002	0.244	0.862	0.950	0.059	1.119
	10	3.646	0.507	2.797	6.044	6.866	12.692	13.329
	20	3.614	0.228	3.446	3.450	4.052	5.721	6.040
	30	4.345	0.186	3.889	2.673	3.145	4.651	4.469
Halloysite	5	0.490	0.148	1.294	6.072	6.693	3.714	10.67
	10	0.215	0.024	0.857	1.609	1.795	0.618	2.668
	20	3.592	0.249	3.334	3.666	4.377	6.229	6.586
	30	1.022	0.047	2.012	1.526	1.744	1.181	2.338

Table 5 Intraparticle diffusion kinetic model of adsorption of MB onto halloysite and kaolinite

[MB]$_{ini}$ (mg/L)	Halloysite						Kaolinite					
	K_{id1}	Intercept	R^2	K_{id2}	Intercept	R^2	K_{id1}	Intercept	R^2	K_{id2}	Intercept	R^2
5	0.04	4.55	0.83	0.00	4.88	NA	0.30	2.53	0.88	0	4.22	NA
10	0.71	5.84	0.99	0.01	9.42	0.79	0.22	8.03	0.96	0	9.33	NA
20	1.01	12.84	0.99	0.02	18.92	NA	0.85	12.39	0.85	0	16.74	NA
30	0.88	21.08	0.87	0.05	25.87	0.98	0.41	20.45	0.78	0	22.78	NA

all of the R^2 values are around 0.90 pointing out the good applicability of Weber's intraparticle diffusion model for MB adsorption onto the HNTs and kaolinite.

4 Conclusion

High adsorptive capacity of raw kaolinite-rich clay for MB was highlighted through this study. Raw halloysite displays higher MB absorption capacities than raw kaolinite/illite. The equilibrium adsorption capacity of methylene blue increased with temperature and the increase in initial concentration of MB. pH plays a key role in this process. Adsorption is dominantly by a tow-step intraparticle diffusion process, and the adsorption kinetics could be well adjusted by a pseudo-second-order kinetic equation.

Our results indicate that a raw kaolinite/illite and halloysite samples can be successfully utilized for the adsorption of methylene blue dye from aqueous solutions. Raw halloysite has higher adsorption capacity of MB than kaolinite. The thermodynamic parameters show that the sorption of MB is spontaneous ($\Delta G < 0$) and endothermic ($\Delta H > 0$) for halloysite, while the sorption of kaolinite is thermodynamically unfavorable ($\Delta G > 0$) and the adsorption of MB is inhibited by electrostatic exothermic effects ($\Delta H < 0$). The intraparticle diffusion process controls the adsorption reaction, and the kinetic is more important for halloysite.

Compliance with ethical standards

Conflict of interest statement No conflicts of interest to declare.

References

1. Mondal S (2008) Methods of dye removal from dye house effluent-an overview. Environ Eng Sci 25:383–396. https://doi.org/10.1089/ees.2007.0049
2. Gupta VK, Carrott PJM, Ribeiro Carrott MML et al (2009) Low-cost adsorbents: growing approach to wastewater treatment-a review. Crit Rev Environ Sci Technol 39:783–842. https://doi.org/10.1080/10643380801977610
3. Yagub MT, Sen TK, Afroze S et al (2014) Dye and its removal from aqueous solution by adsorption: a review. Adv Coll Interface Sci 209:172–184. https://doi.org/10.1016/j.cis.2014.04.002
4. Ngulube T, Gumbo JR, Masindi V et al (2017) An update on synthetic dyes adsorption onto clay based minerals: a state-of-art review. J Environ Manag 191:35–57. https://doi.org/10.1016/j.jenvman.2016.12.031
5. Aghdasinia H, Asiabi HR (2018) Adsorption of a cationic dye (methylene blue) by Iranian natural clays from aqueous solutions: equilibrium, kinetic and thermodynamic study. Environ Earth Sci 77:218. https://doi.org/10.1007/s12665-018-7342-5
6. Sarici-Özdemir Ç, Kiliç F (2018) Kinetics behavior of methylene blue onto agricultural waste. Part Sci Technol 36:194–201. https://doi.org/10.1080/02726351.2016.1240127
7. Sarici Özdemir Ç (2019) Equilibrium, kinetic, diffusion and thermodynamic applications for dye adsorption with pine cone. Sep Sci Technol 54:3046–3054. https://doi.org/10.1080/01496395.2019.1565769
8. Tamai H, Yoshida T, Sasaki M et al (1999) Dye adsorption on mesoporous activated carbon fiber obtained from pitch containing yttrium complex. Carbon 37:983–989. https://doi.org/10.1016/S0008-6223(98)00294-2
9. Wang S, Li H, Xu L (2006) Application of zeolite MCM-22 for basic dye removal from wastewater. J Colloid Interface Sci 295:71–78. https://doi.org/10.1016/j.jcis.2005.08.006
10. Maffei AV, Budd PM, McKeown NB (2006) Adsorption studies of a microporous phthalocyanine network polymer. Langmuir 22:4225–4229. https://doi.org/10.1021/la060091z
11. Wu FC, Tseng RL, Juang RS (2005) Preparation of highly microporous carbons from fir wood by KOH activation for adsorption of dyes and phenols from water. Sep Purif Technol 47:10–19. https://doi.org/10.1016/j.seppur.2005.03.013
12. Shukla S, Dhiman N (2017) Characterization and adsorption of disperse dyes from wastewater onto cenospheres activated carbon composites. Environ Earth Sci 76:702. https://doi.org/10.1007/s12665-017-7030-x
13. Lee CK, Lin KS, Wu CF et al (2008) Effects of synthesis temperature on the microstructures and basic dyes adsorption of titanate nanotubes. J Hazard Mater 150:494–503. https://doi.org/10.1016/j.jhazmat.2007.04.129
14. Chen Z, Zhang J, Fu J, Wang M, Wang X, Han R, Xu Q (2014) Adsorption of methylene blue onto poly (cyclotriphosphazene-co-4, 4'-sulfonyldiphenol) nanotubes: kinetics, isotherm and thermodynamics analysis. J Hazard Mater 273:263–271
15. Chen Z, Fu J, Wang M, Wang X, Zhang J, Xu Q (2014) Adsorption of cationic dye (methylene blue) from aqueous solution using poly (cyclotriphosphazene-co-4, 4'-sulfonyldiphenol) nanospheres. Appl Surf Sci 289:495–501
16. Fu J, Chen Z, Wang M, Liu S, Zhang J, Zhang J, Runping H, Xu Q (2015) Adsorption of methylene blue by a high-efficiency adsorbent (polydopamine microspheres): kinetics, isotherm, thermodynamics and mechanism analysis. Chem Eng J 259:53–61
17. Murray HH (2000) Traditional and new applications for kaolin, smectite, and palygorskite: a general overview. Appl Clay Sci 17:207–221. https://doi.org/10.1016/S0169-1317(00)00016-8
18. Crini G (2006) Non-conventional low-cost adsorbents for dye removal: a review. Biores Technol 97:1061–1085. https://doi.org/10.1016/j.biortech.2005.05.001
19. Mouni L, Belkhiri L, Bollinger JC et al (2018) Removal of methylene blue from aqueous solutions by adsorption on kaolin: kinetic and equilibrium studies. Appl Clay Sci 153:38–45. https://doi.org/10.1016/j.clay.2017.11.034
20. Bailey SW (1963) Polymorphism of the kaolin minerals. American Mineralogist. J Earth Planet Mater 48:1196–1209
21. Dill HG (2016) Kaolin: soil, rock and ore: from the mineral to the magmatic, sedimentary and metamorphic environments. Earth Sci Rev 161:16–129. https://doi.org/10.1016/j.earscirev.2016.07.003
22. Ma C, Eggleton RA (1999) Cation exchange capacity of kaolinite. Clays Clay Miner 47:174–180. https://doi.org/10.1346/CCMN.1999.0470207
23. Ōya A, Kizu K, Ōtani S (1987) Porous materials prepared by heating derivatives from halloysite. J Mater Sci 22:4541–4545. https://doi.org/10.1007/BF01132060
24. Zhou CH, Keeling J (2013) Fundamental and applied research on clay minerals: from climate and environment to

nanotechnology. Appl Clay Sci 74:3–9. https://doi.org/10.1016/j.clay.2013.02.013

25. El Haddar A, Gharibi E, Azdimousa A et al (2018) Characterization of halloysite (North East Rif, Morocco): evaluation of its suitability for the ceramics industry. Clay Miner 53:65–78. https://doi.org/10.1180/clm.2018.5

26. Shu Z, Chen Y, Zhou J et al (2015) Nanoporous-walled silica and alumina nanotubes derived from halloysite: controllable preparation and their dye adsorption applications. Appl Clay Sci 112:17–24

27. Levis SR, Deasy PB (2002) Characterisation of halloysite for use as a microtubular drug delivery system. Int J Pharm 243:125–134. https://doi.org/10.1016/S0378-5173(02)00274-0

28. Massaro M, Colletti CG, Lazzara G et al (2017) Halloysite nanotubes as support for metal-based catalysts. J Mater Chem A 5:13276–13293. https://doi.org/10.1039/C7TA02996A

29. Maziarz P, Matusik J (2016) The effect of acid activation and calcination of halloysite on the efficiency and selectivity of Pb(II), Cd (II), Zn (II) and As (V) uptake. Clay Miner 51:385–394. https://doi.org/10.1180/claymin.2016.051.3.06

30. Anastopoulos I, Mittal A, Usman M et al (2018) A review on halloysite-based adsorbents to remove pollutants in water and wastewater. J Mol Liq 269:855–868. https://doi.org/10.1016/j.molliq.2018.08.104

31. Ngulube T, Gumbo JR, Masindi V et al (2019) Evaluation of the efficacy of halloysite nanotubes in the removal of acidic and basic dyes from aqueous solution. Clay Miner 54:197–207

32. Dahmani H, Jadid M, El Hammouti K et al (2016) The origin of Kaolin in the Béni-Snassène granodiorite sand (Northeastern Morocco). J Mater Environ Sci 7:4723–4732

33. Rouiller J, Souchie B, Bruckert S et al (1994) Méthodes d'analyses des sols. In: Bonneau M, Souchier B (eds) Pédologie: 2. Constituants et propriétés du sol. Paris, Masson, p 459

34. Mantin I (1969) Mesure de la capacité d'échange des minéraux argileux par l'éthylène diamine et les ions complexes de l'éthylène diamine. Comptes Rendus des Séances de l'Académie des Sciences, Série D: Sciences Naturelles 269:815–818

35. Bergaya F, Vayer M (1997) CEC of clays: measurement by adsorption of a copper ethylenediamine complex. Appl Clay Sci 12:275–280. https://doi.org/10.1016/S0169-1317(97)00012-4

36. Doğan M, Alkan M (2003) Adsorption kinetics of methyl violet onto perlite. Chemosphere 50:517–528. https://doi.org/10.1016/S0045-6535(02)00629-X

37. Alkan M, Demirbaş Ö, Doğan M (2007) Adsorption kinetics and thermodynamics of an anionic dye onto sepiolite. Microporous Mesoporous Mater 101:388–396. https://doi.org/10.1016/j.micromeso.2006.12.007

38. Shaker MA (2014) Dynamics and thermodynamics of toxic metals adsorption onto soil-extracted humic acid. Chemosphere 111:587–595. https://doi.org/10.1016/j.chemosphere.2014.04.088

39. Yu F, Sun S, Han S et al (2016) Adsorption removal of ciprofloxacin by multi-walled carbon nanotubes with different oxygen contents from aqueous solutions. Chem Eng J 285:588–595. https://doi.org/10.1016/j.cej.2015.10.039

40. Bordeepong S, Bhongsuwan D, Pungrassami T et al (2011) Characterization of halloysite from Thung Yai District, Nakhon Si Thammarat Province, in Southern Thailand, Songklanakarin. J Sci Technol 33:599–607

41. Ouyang J, Zhou Z, Zhang Y et al (2014) High morphological stability and structural transition of halloysite (Hunan, China) in heat treatment. Appl Clay Sci 101:16–22. https://doi.org/10.1016/j.clay.2014.08.010

42. Lu Y, Wang R, Lu X et al (2016) Reprint of Genesis of halloysite from the weathering of muscovite: insights from microscopic observations of a weathered granite in the Gaoling Area, Jingdezhen, China. Appl Clay Sci 119:59–66. https://doi.org/10.1016/j.clay.2015.08.024

43. Van der Marel HW, Beutelspacher H (1976) Atlas of infrared spectroscopy of clay minerals and their admixtures. Elsevier, Dordrecht

44. Joussein E, Petit S, Churchman J, Theng B, Righi D, Delvaux B (2005) Halloysite clay minerals—a review. Clay Miner 4:383–426. https://doi.org/10.1180/0009855054040180

45. Özdemir Y, Doğan M, Alkan M (2006) Adsorption of cationic dyes from aqueous solutions by sepiolite. Microporous Mesoporous Mater 96:419–427. https://doi.org/10.1016/j.micromeso.2006.07.026

46. Shchukin DG, Lamaka SV, Yasakau KA et al (2008) Active anticorrosion coatings with halloysite nanocontainers. J Phys Chem C 112:958–964. https://doi.org/10.1021/jp076188r

47. Kretzschmar R, Holthoff H, Sticher H (1998) Influence of pH and humic acid on coagulation kinetics of kaolinite: a dynamic light scattering study. J Colloid Interface Sci 202:95–103. https://doi.org/10.1006/jcis.1998.5440

48. Huertas FJ, Chou L, Wollast R (1999) Mechanism of kaolinite dissolution at room temperature and pressure Part II: kinetic study. Geochim Cosmochim Acta 63:3261–3275. https://doi.org/10.1016/S0016-7037(99)00249-5

49. Stumm W (1987) Aquatic surface chemistry: chemical processes at the particle-water interface. Wiley, New York

50. Wu CH (2007) Adsorption of reactive dye onto carbon nanotubes: equilibrium, kinetics and thermodynamics. J Hazard Mater 144:93–100. https://doi.org/10.1016/j.jhazmat.2006.09.083

51. Omer OS, Hussein MA, Hussein BH et al (2018) Adsorption thermodynamics of cationic dyes (methylene blue and crystal violet) to a natural clay mineral from aqueous solution between 293.15 and 323.15 K. Arab J Chem 11:615–623. https://doi.org/10.1016/j.arabjc.2017.10.007

52. Kara M, Yuzer H, Sabah E et al (2003) Adsorption of cobalt from aqueous solutions onto sepiolite. Water Res 37:224–232. https://doi.org/10.1016/S0043-1354(02)00265-8

53. Ward DB, Brady PV (1998) Effect of Al and organic acids on the surface chemistry of kaolinite. Clays Clay Miner 46:453–465. https://doi.org/10.1346/CCMN.1998.0460410

54. Taty-Costodes VC, Fauduet H, Porte C et al (2003) Removal of Cd (II) and Pb(II) ions, from aqueous solutions, by adsorption onto sawdust of Pinus sylvestris. J Hazard Mater 105:121–142. https://doi.org/10.1016/j.jhazmat.2003.07.009

55. Ho YS, McKay G (1998) Sorption of dye from aqueous solution by peat. Chem Eng J 70:115–124. https://doi.org/10.1016/S0923-0467(98)00076-1

56. Kumar KV, Porkodi K, Rocha F (2008) Comparison of various error functions in predicting the optimum isotherm by linear and non-linear regression analysis for the sorption of basic red 9 by activated carbon. J Hazard Mater 150:158–165. https://doi.org/10.1016/j.jhazmat.2007.09.020

57. Doğan M, Alkan M, Türkyilmaz A et al (2004) Kinetics and mechanism of removal of methylene blue by adsorption onto perlite. J Hazard Mater 109:141–148. https://doi.org/10.1016/j.jhazmat.2004.03.003